Astronomy & Astrophysics manuscript no. aa5401
February 5, 2008

The distribution of ND_2H in LDN1689N

M. Gerin[1], D.C. Lis[2], S. Philipp[3], R. Güsten[3], E. Roueff[4], and V. Reveret[5]

[1] LERMA, CNRS UMR8112, Observatoire de Paris and ENS , 24 Rue Lhomond, 75231 Paris cedex 05 France, e-mail: gerin@lra.ens.fr
[2] California Institute of Technology, MC 320-47, Pasadena, CA 91125 , USA, e-mail: dcl@submm.caltech.edu
[3] Max Planck Institut für Radioastronomie, Auf dem Hügel 69, Bonn, Germany, e-mail: philipp,guesten@mpifr-bonn.mpg.de
[4] LUTH, CNRS UMR8102, Observatoire de Paris and Université Paris 7, Place J. Janssen, 92190 Meudon, France , e-mail: evelyne.roueff@obspm.fr
[5] European Southern Observatory, Casilla 19001, Santiago 19, Chile, e-mail: vreveret@eso.org

Received 10 April 2006 / Accepted 01 June 2006

ABSTRACT

Aims. Finding tracers of the innermost regions of prestellar cores is important for understanding their chemical and dynamical evolution before the onset of gravitational collapse. While classical molecular tracers, such as CO and CS, have been shown to be strongly depleted in cold, dense gas by condensation on grain mantles, it has been a subject of discussion to what extent nitrogen-bearing species, such as ammonia, are affected by this process. As deuterium fractionation is efficient in cold, dense gas, deuterated species are excellent tracers of prestellar cores. A comparison of the spatial distribution of neutral and ionized deuterated species with the dust continuum emission can thus provide important insights into the physical and chemical structure of such regions.

Methods. We study the spatial distribution of the ground-state 335.5 GHz line of ND_2H in LDN1689N, using APEX, and compare it with the distribution of the DCO^+(3–2) line, as well as the 350 μm dust continuum emission observed with the SHARC II bolometer camera at CSO.

Results. While the distribution of the ND_2H emission in LDN1689N is generally similar to that of the 350 μm dust continuum emission, the peak of the ND_2H emission is offset by $\sim 10''$ to the East from the dust continuum and DCO^+ emission peak. ND_2H and ND_3 share the same spatial distribution. The observed offset between the ND_2H and DCO^+ emission is consistent with the hypothesis that the deuterium peak in LDN1689N is an interaction region between the outflow shock from IRAS16293–2422 and the dense ambient gas. We detect the $J = 4 \rightarrow 3$ line of $H^{13}CO^+$ at 346.998 GHz in the image side band serendipitously. This line shows the same spatial distribution as DCO^+(3–2), and peaks close to the 350 μm emission maximum which provides further support for the shock interaction scenario.

Key words. Interstellar medium – molecules – individual objects : LDN1689N

1. Introduction

Deuteration of nitrogen compounds, such as ammonia and N_2H^+, is spectacular in a number of environments including dark clouds, such as L134N (Tiné et al. 2000; Roueff et al. 2000; Roueff et al. 2005), low-mass star forming regions and prestellar cores such as LDN1689N and Barnard 1 (Loinard et al. 2001; Gerin et al. 2001; Lis et al. 2002a). The discussion of the respective contributions of grain and gas-phase processes in the deuteration is active, but no definite solution is yet available. The lack of detection of deuterated water in ices toward low-mass young stellar objects (YSOs) by Dartois et al. (2003) and Parise et al. (2003) suggests that "another mechanism than pure solid state chemistry may be active to produce very high deuterium enrichment in the gas phase."

Further constraints on the deuterium fractionation mechanisms are provided by the spatial distribution of deuterated species, as compared with the molecular gas distribution traced by the submillimeter dust continuum emission. Whereas maps of singly deuterated species have been published in many cores — the relatively large line intensities of e.g. DCO^+, N_2D^+ allow easy mapping with state of the art detectors — mapping multiply deuterated species has proven to be a challenge, given the relatively low line intensities. Ceccarelli et al. (2001) have shown that the D_2CO emission is extended around the class 0 protostar IRAS16293–2422. Roueff et al. (2005) present a limited map of the ND_3 ground-state transition at 309 GHz with the CSO in LDN1689N, which unfortunately suffers from rather poor pointing accuracy. Because the ground state ND_2H $1_{0,1}-0_{0,0}$ lines, at 335.5 for the ortho species and 335.4 GHz for the para species (See Coudert and Roueff (2006) for NH_3 and its isotopologues line frequencies), are relatively strong (0.6 K in LDN1689N; Lis et al. 2006) and the atmospheric transmission is good at this frequency, we have carried out the first map of a doubly deuterated species in a dense core.

Send offprint requests to: M. Gerin

2. Observations

The observations have been carried out using the APEX-2a 350 GHz receiver of the Atacama Pathfinder Experiment (APEX [1]). We combined data obtained during two periods, August 2005 and October 2005. The receiver was tuned in DSB with the ND_2H lines in the lower sideband. The backend was the facility MPIfR Fast Fourier Spectrometer. We observed a total of 10 positions towards LDN1689N (α_{2000} = 16:32:29.470, δ_{2000} = –24:28:52.60). The pointing was checked regularly and found accuracte to $\sim$ 2 – 3″. The observations have been taken in the position-switched mode with a reference position located 240″ East of the source for the August 2005 data. The October 2005 data have been taken with a reference position offset by 10′ in azimuth. Line and continuum maps shown in Lis et al. (2002b) and Stark et al. (2004) show that the source emission rapidly drops towards the East.

The data have been corrected for the sideband gain and the APEX main beam efficiency of 0.7 at 335 GHz. The temperature scale used in this paper is the main beam brightness temperature scale. Overall, the data calibration agree well with the CSO spectrum presented by Lis et al. (2006). The FWHM beam size of APEX is 18″ at 335.5 GHz.

3. Results

Fig. 1 shows the average spectrum integrated over the map, while contour maps are shown in Fig. 2. The ortho- and para-$ND_2H(1_{11}-0_{00})$ lines are clearly detected with a mean intensity ratio of 2:1, reproducing the ortho-to-para statistical weight ratio (Lis et al. 2006). We have also detected the $H^{13}CO^+$(4–3) line at 346.998 GHz in the image side band, which is discussed below.

3.1. ND_2H spatial distribution

Fig. 2 shows contours of the main ND_2H emission at 335.5 GHz (in white) overlayed over a 350 μm continuum image. The ND_2H emission is clearly extended and shows an elongated shape generally similar to the dust continuum emission. The limited ND_3 map shown by Roueff et al. (2005) shows the same elongated pattern. Over the limited extend of the ND_2H map, the line and continuum emissions are positively correlated with a correlation coefficient of 0.29. This rather weak correlation is due to the difference in peak positions of the ND_2H line emission with respect to the continuum peak, the ND_2H emission beeing offset by $\sim$10″ to the East of the dust contimuum emission maximum. This offset far exceeds the pointing uncertainties ($\sim$2 – 3″).

The right panel in Fig. 2 shows an overlay of the ND_2H contours on a DCO^+(3–2) map (Lis et al. 2002b). The ND_2H peak is clearly offset from the DCO^+ peak too. D_2CO (Ceccarelli et al. 2000), ND_3 (Roueff et al. 2005), ND_2H (Loinard et al. 2001, Roueff et al. 2005), DCO^+ (Lis et al; 2002b), all appear at a blueshifted velocity compared to the cloud envelope : V_{LSR} = 3.4 – 3.6 kms^{-1} versus V_{LSR} = 3.8 – 4.0 kms^{-1} for $C^{18}O$ and $C^{17}O$ (Stark et al. 2004). This velocity difference was first recognized by Lis et al. (2002b) who suggested that it results from the shock interaction of the powerful blue lobe of the IRAS16293-2422 outflow with the dense core. The blue lobe of the molecular outflow is interacting and compressing LDN1689N, creating dense and cold post-shock gas, blueshifted relative to the cloud envelope. The deuterated species preferably sample this cold and dense material as deuterium fractionation is more efficient at low temperatures and high gas densities. The large-scale CO and continuum maps presented by Lis et al. (2002b) and Stark et al. (2004) present convincing evidence for this scenario.

The spatial offset between DCO^+ and ND_2H provides additional support for the C-shock hypothesis. The DCO^+ ion is detected ahead of the neutral species ND_2H, closer to IRAS16293-2422. The spatial separation, 10″, or $\sim$0.01 pc, is consistent with C-shock models with a pre-shock density of 10^4 cm^{-3} and a magnetic field of 30 μG (Lesaffre et al. 2004), which predict a total shock size of 0.04 pc. The deuterium chemistry in shocks has been previously studied by Pineau des Forêts et al. (1989) and Bergin et al. (1999) in different contexts. Because of the sensitivity of deuterium fractionation to both the gas temperature and the molecular depletion, it is expected that DCO^+ will be reformed more rapidly than ND_2H in the post-shock gas. While DCO^+ is formed as soon as the gas temperature drops, efficient ND_2H formation requires both cold temperatures and significant CO depletions, which are expected to occur downstream (Bergin et al. 1999). A spatial offset could therefore exist between abundance peaks of DCO^+ and ND_2H, as we have detected. More detailed shock models, would be able to further test the validity of this scenario.

3.2. ND_2H abundance

We have fitted the ND_2H spectra using the hyperfine fitting command in CLASS. Although the signal-to-noise ratio is not high enough for securely deriving the line opacity at all positions, it is clear that the maximum opacity coincides with the maximum signal. The opacity derived for the average of all positions excluding (10″,0″) is 0.2 ± 0.48, and the corresponding excitation temperature is 8 ± 3 K, in good agreement with Lis et al. (2006). The spectra show some indication of higher line opacity, and lower excitation temperature (τ = 3.11 ± 1.5; T_{ex} = 5 ± 1 towards the two positions with highest intensities (0,-10″) and (0,-20″).

The ND_2H column densities have been derived assuming optically thin emission, LTE and using a uniform excitation temperature of 5 K. They are listed, together with the H_2 column density derived from dust continuum measurements in Table 1. We use the 350 μm dust continuum map obtained with SHARC II at the CSO (Fig. 2), and a a dust opacity of κ_{350} = 0.07 cm^{2}g^{-1} corresponding to κ_{1300} = 0.005 cm^{2}g^{-1} (Ossenkopf & Henning 1994) for a dust emissivity index β = 2, and a dust temperature of 16 K (Stark et al. 2004). The 350 μm continuum fluxes are in fair agreement with the values reported

[1] This publication is based on data acquired with the Atacama Pathfinder Experiment (APEX). APEX is a collaboration between the Max-Planck-Institut für Radioastronomie, the European Southern Observatory and the Onsala Space Observatory.

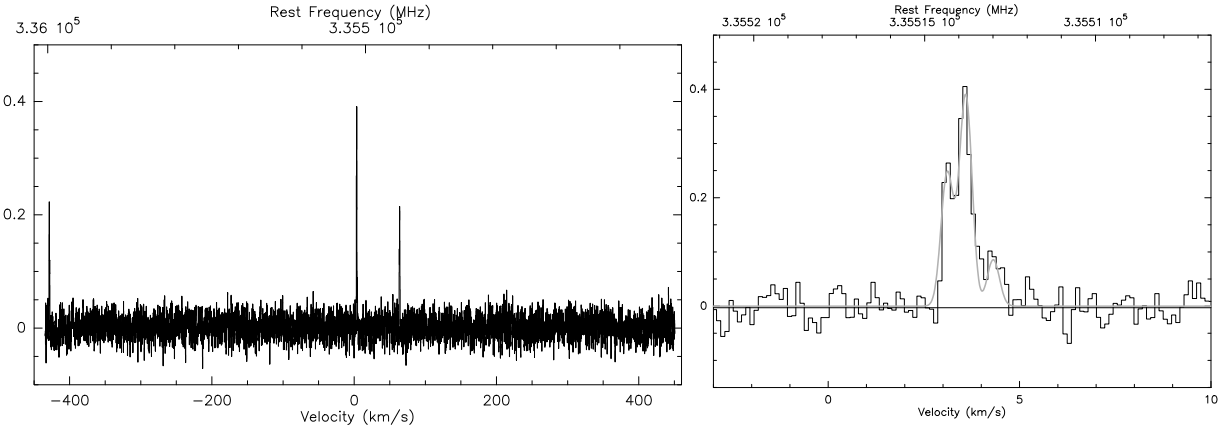

Fig. 1. Left : Full spectrum averaged over the map. p-$ND_2H(1_{11} - 0_{00})$ at 335.446 GHz, o-$ND_2H(1_{11} - 0_{00})$ at 335.514 GHz and $H^{13}CO^+$(4–3) at 346.998 GHz (in the image side band) are detected. Right : Enlargement showing a fit of the hyperfine structure of the o-ND_2H line. The temperature scale is $T_{\rm mb}$ (K) and the velocity scale is relative to the LSR.

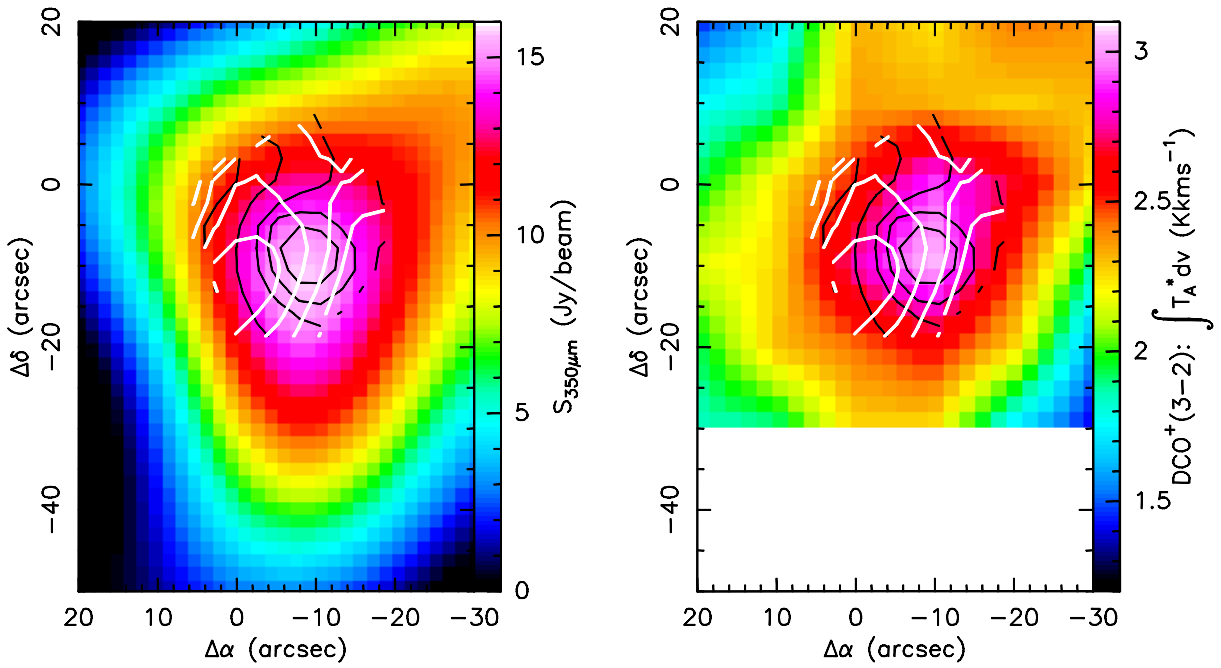

Fig. 2. Left: Color image of the 350 μm dust continuum emission obtained with SHARC II at the CSO, convolved to 20″ angular resolution. The intensity scale is given in Jy/beam. White contours show the integrated intensity of the o-ND_2H line at 335.5 GHz, with contour levels from 0.25 to 0.45 Kkms^{-1} with 0.05 Kkms^{-1} spacing. Black contours show the integrated intensity of the $H^{13}CO^+$(4–3) line at 346.998 GHz, with contour levels from 0.25 to 0.87 Kkms^{-1} with 0.125 Kkms^{-1} spacing. The map center is α_{2000} = 16:32:29.470, δ_{2000} = -24:28:52.60. Right: The same contours plotted on a DCO^+(3–2) map (Lis et al. 2002b).

by Stark et al. (2004), but on the lower side: we detect a maximum intensity of 16 Jy in a 20” beam, to be compared with 19.4 ± 2.3 Jy in Stark et al. (2004). This dicrepancy may be an indication that some low-level entended emission is filtered out in the SHARC II image, which has been obtained in the “AC-biased mode”, without the secondary chopper. The resulting H_2 column densities reported in Table 1 could therefore be affected by this 35% uncertainty.

The H_2 column density ranges from 3.1×10^{22} cm^{-2} to $7.2{\times}10^{22}$ cm^{-2} across the map. The corresponding ND_2H abundances varies from 0.7×10^{-9} to 2.6×10^{-9} relative to H_2, with a mean value of 1.8×10^{-9}, in good agreement with previous work (Lis et al. 2006). ND_2H appears to be remarkably abundant in this dense core. For the three positions where reliable ND_3 data exist (Roueff et al. 2005), the $[ND_3]/[ND_2H]$ abundance ratio is 0.01 – 0.02, and seems to increase with increasing ND_2H column density.

3.3. $H^{13}CO^+$

A relatively strong line is detected at the lower end of the velocity range in Fig. 1. Careful tests have been performed using the CSO and APEX telescopes for identifying this line. It turns out that the line can be assigned to the $J = 4 \rightarrow 3$ transi-

Table 1.

Position (arcsec)	V kms^{-1}	δV kms^{-1}	$N(ND_2H)^1$ 10^{13} cm^{-2}	$N(ND_3)^2$ 10^{12} cm^{-2}	$N(H_2)^3$ 10^{22} cm^{-2}
-10,10	3.63 ± 0.02	0.33 ± 0.03	9.8 ± 2		4.1 ± .5
10,0	3.53 ± 0.02	0.20 ± 0.07	3.6 ± 1		3.1 ± .5
0,0	3.56 ± 0.02	0.40 ± 0.05	12.7 ± 2	1.5	5.1 ± .5
-10,0	3.62 ± 0.02	0.39 ± 0.05	10.0 ± 2		5.9 ± .5
-20,0	3.75 ± 0.1	0.8 ± 0.3	8.9 ± 2		5.4 ± .5
0, -10	3.60 ± 0.02	0.30 ± 0.05	15.8 ± 2		5.8 ± .5
-10,-10	3.70 ± 0.05	0.55 ± 0.1	11.7 ± 2	1.8	7.1 ± .5
-20,-10	3.55 ± 0.02	0.26 ± 0.05	4.6 ± 1		5.7 ± .5
0,-20	3.69 ± 0.02	0.45 ± 0.06	12.7 ± 2	2.6	5.2 ± .5
-10,-20	3.72 ± 0.03	0.58 ± 0.08	8.9 ± 2		6.5 ± .5

[1] Derived assuming LTE and T_{ex} = 5 K. [2] Roueff et al. (2005).[3] Derived assuming T_{dust} = 16 K and κ_{350} = 0.07 cm^2g^{-1}.

tion of $H^{13}CO^+$ at 346.998 GHz seen in the image side band. At APEX, when the system is tuned to ND_2H, the $H^{13}CO^+$ line falls 16MHz outside the 1GHz wide IF band, but is aliased back into the signal band. The band edge IF filter attenuates the line intensity, therefore the correct intensity scale has been established by comparing the original data with additional measurements taken with APEX on May 22nd, 2006 with the $H^{13}CO^+$ line centered in the signal band. The 2005 data have been multiplied by 2.5 to match the properly tuned 2006 data. We have checked that the spatial distributions of $H^{13}CO^+$(4-3) agree reasonably well between both datasets. $H^{13}CO^+$(4–3) has a more sharply peaked spatial distribution than ND_2H (Fig. 2), which is very similar to the DCO^+(3–2) map obtained at the CSO (see right panel of Fig. 2).

4. Conclusions

1. We show that the ND_2H emission is extended in the LDN1689N dense core. The abundance relative to H_2, derived from LTE, is $\sim 1.8 \times 10^{-9}$, which makes ND_2H a remarkably abundant molecule in this dense core. The $[ND_3]/[ND_2H]$ abundance ratio is 0.01 – 0.02.
2. The ND_2H emission is spatially offset from the dust continuum DCO^+(3–2) and $H^{13}CO^+$(4–3) emission by $\sim$ 0.01 pc, and appears to be blueshifted relative to the cloud envelope. Both findings are qualitatively consistent with the scenario of the formation of the LDN1689N dense core by the interaction of the blue lobe of the IRAS16293–2422 molecular outflow with the ambient material. Detailed models could further test this scenario.

Acknowledgements. Caltech Submillimeter Observatory is supported by the U.S. National Science Foundation, grant AST 0540882. We thank the MPG and ESO APEX teams for their support, especially P. Bergman and L.- Å. Nyman.

References

Bergin E.A., Neufeld D.A., Melnick G.J., 1999, ApJ 510, L145.
Ceccarelli C., Vastel C., Tielens A.G.G.M., et al., 2000, A&A 381, L17.
Ceccarelli, C., Loinard, L., Castets, A., Tielens, A. G. G. M., Caux, E., Lefloch, B., Vastel, C., A&A 372, 998.
Coudert L.H., Roueff,E., 2006, A&A 449, 855.
Dartois, E., Thi, W.-F., Geballe, T. R., Deboffle, D., d'Hendecourt, L., van Dishoeck, E., 2003, A&A 399, 1009
Gerin, M., Pearson, J. C., Roueff, E., Falgarone, E., Phillips, T. G., 2001, ApJ 551, L193
Lesaffre P., Chièze J.P., Cabrit S., Pineau des Forêts G., 2004, A&A 427, 147.
Lis, D. C., Roueff, E., Gerin, M., Phillips, T. G., Coudert, L. H., van der Tak, F. F. S., Schilke, P, 2002a, ApJ 571, L55
Lis, D. C., Gerin, M., Phillips, T. G., Motte, F., 2002b, ApJ 569, 322.
Lis, D.C., Gerin, M., & Roueff, E. 2006, ApJ 636, 916
Loinard, L., Castets, A., Ceccarelli, C., Caux, E., Tielens, A. G. G. M., 2001, ApJ 552 L163
Parise, B., Simon T., Caux, E., Dartois, E., Ceccarelli, C., Rayner, J., Tielens, A. G. G. M., 2003, A&A 410, 897
Ossenkopf V., Henning T., 1994, A&A 291, 943
Pineau des Forêts G., Roueff E., Flower D.R., 1989, MNRAS 240, 167.
Roueff, E., Tiné, S., Coudert, L. H., Pineau des Forêts, G., Falgarone, E., Gerin, M., A&A 354, L63
Roueff, E., Lis, D. C., van der Tak, F. F. S., Gerin, M., Goldsmith, P. F., 2005, A&A, 438, 585
Stark, R., Sandell, G., Beck, S. C., et al., 2004, ApJ 608, 341
Tiné, S., Roueff, E., Falgarone, E., Gerin, M., Pineau des Forêts, G., 2000, A&A 356, 1039

List of Objects